No.

国立天文台 天文学データ解析計算センター
成果報告書 (平成17年度)

提出期限：平成18年3月20日(月)17:00必着

応募カテゴリ（いずれかを選択）　A
システム（いずれかを選択）　VPP

プロジェクト ID: wna15b

研究代表者（現在のユーザID：arimtonb）

氏名	有本 信雄
所属機関名	国立天文台
連絡先住所	〒 181-8588 東京都三鷹市大沢 2-21-1
電話番号	0422-34-3515
E–mail	arimoto@optik.mtk.nao.ac.jp
職または学年	教授
研究代表者が学生の場合には指導教官の氏名	

研究課題名

(和文)	矮小銀河形成数値シミュレーション
(英文)	Numerical Simulations of Dwarf Galaxy Formation

研究分担者

氏名	所属機関名	E–mail	ユーザID
河田 大介	Carnegie Observatories	dkawata@ociw.edu	kawatads

成果に関連して出版、もしくは印刷、投稿中の論文リスト

(1) このプロジェクト（同様の過去のプロジェクトも含む）での成果

今年度中に出版された論文、国際会議集録、国際会議、学会、研究会発表、その他出版物（印刷中、投稿中の場合はその旨を記載すること）

学術論文

D. Kawata, **N. Arimoto**, R. Cen, B.K. Gibson,
Origin of Two Distinct Populations in Dwarf Spheroidal Galaxies, ApJ in press.

(2) これまでのプロジェクトの今年度中の成果

今年度中に出版された論文、国際会議集録、国際会議、学会、研究会発表、その他出版物（印刷中、投稿中の場合はその旨を記載すること）

※ 評価資料として利用いたしますので、様式・順序は任意ですが、学術論文については題名、著者、発行年月、雑誌名、巻、ページが記載されていること。

特に無し.

成果の概要

Abstract

We study the chemical and kinematic properties of the first galaxies which formed at a high redshift, using high resolution cosmological numerical simulations, and compared them with the recent observational results for the Sculptor dwarf spheroidal galaxy by Tolstoy et al., who found two distinct stellar populations: the lower metallicity stars are more spatially extended and possess a higher velocity dispersion than the higher metallicity stars. Our calculations reproduce these observations as the result of a steep metallicity gradient, within a single populations, induced by dissipative collapse of the gas component. We also predict strong [N/O] enhancements in the lowest metallicity stars in dwarf spheroidals, due to the preferential retention of ejected gas from intermediate mass stars, compared to Type II supernovae.

1. Introduction

Dwarf galaxies in the Local Group are one of the prime observational targets for galactic astronomy, because their relatively short distances enable us to observe the properties of individual stars, which provide great details of their formation history (Baade, 1944). Dwarf Spheroidals (dSphs) are one of the most populous dwarf galaxy type seen in the Local Group, and are defined as galaxies with $M_B > -14$ mag, low surface brightness ($\mu_V > 22$ mag arcsec^{-2}), no well-defined nucleus (although in some dSphs, like Fornax and Sagittarius, a globular cluster seems to correspond to nucleus), and very little gas (Gallagher & Wyse, 1994). They do not have any ongoing star formation. Some of them do not have any intermediate-age stars at all. On the other hand, our current favorite Λ-dominated cold dark matter (ΛCDM) cosmology suggests that small objects form first, and larger systems are built up by the assembly of smaller systems (e.g., White & Rees, 1978). Therefore, it is considered that dSphs might be the first generation of galaxies and survived from cannibalization by larger systems. Hence, dSphs might contain a record of the epoch of the end of the dark age. Recently, using a cosmological numerical simulation, Ricotti & Gnedin (2005) demonstrated that the small galaxies formed at high redshifts can explain the global properties, such as the luminosity, velocity dispersion, and iron abundance, of the dwarf galaxies observed in the Local Group. Their study encourages us to make a further investigation of the connection between the first galaxies and the dSphs.

With the wide field multi-object spectrograph, *FLAMES* on the *Very Large Telescope*, Tolstoy et al. (2004) (T04) have measured the metallicity and line-of-sight velocity for 300 member stars, distributed over a large radial range ($\sim$ 20 times its core radius), in the Sculptor (Scl) dSph galaxy. They found that the stars in the Scl dSph show two distinct populations. One of them is more metal rich ([Fe/H]~ -1.4) with a centrally concentrated distribution. The other one is metal-poor ([Fe/H]~ -2) and more spatially extended. In addition, the higher metallicity stars show lower velocity dispersion than the lower metallicity stars. This is unprecedented information to unveil the formation history of the Scl dSph.

To disentangle the formation process of the dSph from such observational data, we construct a theoretical model which can be compared with the observations. The aim of this paper is to show our first attempt to make a self-consistent numerical simulation model which can be compared with the observational data of the Scl dSph directly and quantitatively. We pay particular attention to the radial trend of iron abundance and velocity dispersion, to compare with the unprecedentedly detailed observation presented in T04, which are not discussed in Ricotti & Gnedin (2005). The next section describes our numerical method. Section 3 presents our simulation results and comparison with the observational data in T04. Discussion and conclusion are seen in Section 4.

2. Numerical Methods

In this study we focus on the properties of a dwarf galaxy which formed at a high redshift in our high resolution cosmological simulation. The simulation was carried out using the galactic chemodynamics code, `GCD+` (Kawata & Gibson, 2003a). `GCD+` is a three-dimensional tree N-body/smoothed particle hydrodynamics (SPH) code which incorporates self-gravity, hydrodynamics, radiative cooling, star formation, supernovae (SNe) feedback, and metal enrichment.

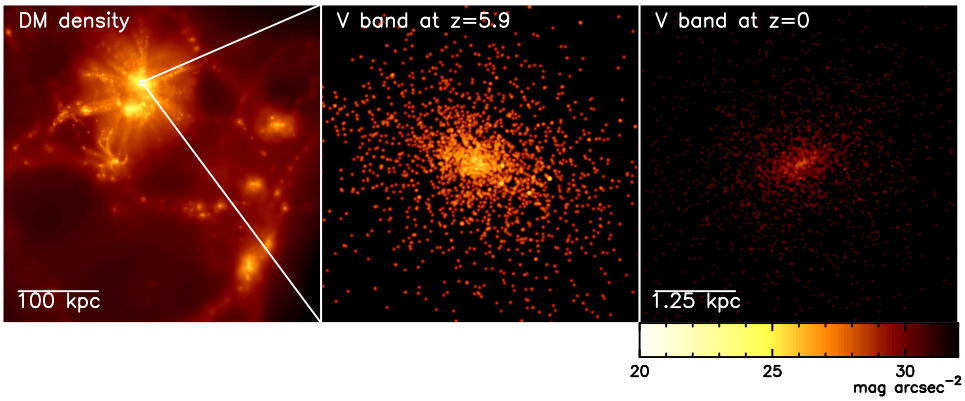

図 1: Dark matter density distribution at $z = 5.9$ (left), V-band (rest-frame) luminosity distribution at $z = 5.9$, and expected V-band luminosity distribution at $z = 0$ after the passive evolution.

GCD+ takes account of the chemical enrichment by both Type II (SNe II) and Type Ia (SNe Ia) SNe, mass-loss from intermediate mass stars, and follows the chemical enrichment history of both the stellar and gas components of the system. To study the formation process of small systems, we update the code to implement non-equilibrium chemical reactions of hydrogen and helium species (H, H^+, He, He^+, He^{++}, H_2, H_2^+, H^-) and their cooling processes.

We adopt a ΛCDM cosmology of $\Omega_0 h^2 = 0.135$, $\Lambda_0 = 1 - \Omega_0$, $\Omega_b h^2 = 0.0224$ and $h = 0.71$, (Spergel et al., 2003), and use a multi-resolution technique (Kawata & Gibson, 2003b) to achieve high-resolution in the regions of interest, while outer regions exerting the tidal forces are handled with lower resolution. The initial conditions for the simulations are constructed using the public software GRAFIC2 (Bertschinger, 2001). Gas dynamics and star formation are included only within the relevant high-resolution region (∼80 kpc in comoving scale); the surrounding low-resolution region (∼530 kpc diameter sphere) contributes to the high-resolution region only through gravity. Consequently, the initial condition consists of total 287,491 dark matter particles and 233,280 gas particles. The mass and softening length of individual gas (dark matter) particles in the high-resolution region are 129 (650) $M_\odot$ and 30 (51) pc, respectively.

To reduce the computational cost, we applied the significantly small simulation volume. Hence, our simulation misses the density perturbation induced by larger scale modes. In addition, the first galaxies are expected to form at high density peaks, i.e. biased regions (Mo & White, 1996). Therefore, we adopt a higher value of $\sigma_8 = 1.8$, instead of a value suggested by recent observations ($\sigma_8 = 0.9$). The adopted high σ_8 value enables us to form a relevant dSph-like small galaxy in the particular realization with the relatively small simulation volume, in addition to partly compensate for the missing waves larger than our simulation box.

In the high-resolution region, we found a small stellar system at $z = 5.9$ (Figure 1). The virial radius and mass of this system are respectively 1.9 kpc and $5.1 \times 10^7 M_\odot$ at $z = 5.9$. Here, we follow the fitting formula in Appendix of Kitayama & Suto (1996) to define the virial mass and radius, taking into account the cosmology and redshift. We assume that at this redshift star formation in this system has been quenched by mechanisms, such as re-ionization (e.g., Efstathiou, 1992) and/or galactic wind (e.g., Dekel & Silk, 1986; Arimoto & Yoshii, 1987), and the system evolves passively afterwards. Thus, we assume that the chemical and kinematic

properties at $z = 5.9$ would not change till $z = 0$, and we analyze the properties expected at $z = 0$ from the output of the simulation at $z = 5.9$. This is, of course, consistent with our assumption that the observed dSph is a galaxy that formed early and retained its own identity until z=0. We will check this ansatz by examining its detailed properties.

The middle panel of Figure 1 shows the rest-frame V-band luminosity distribution of this galaxy at $z = 5.9$. The luminosity distribution is calculated by our population synthesis code, taking account of the metallicity and age of the star particles at $z = 5.9$. We use the single stellar population spectrum data in Kodama & Arimoto (1997). The data do not include any emission lines. For simplicity, we do not take into account any absorption by the inter-stellar (ISM) and inter-galactic medium (IGM). To make sure that the system is dynamically stable and the distribution of stellar population and kinematics does not change till $z = 0$ dramatically, we run a pure N-body simulation using the particles within a radius of ~ 1.7 times the virial radius at $z = 5.9$, as an initial condition. We run this N-body simulation (relaxing run) for about five Gyr (corresponding to the time from $z = 5.9$ to $z = 1$). The right panel of Figure 1 shows the rest-frame V-band luminosity distribution analyzed from the final output of this relaxing run extrapolated at $z = 0$, based on the stellar age at $z = 0$. Figure 2 shows the V-band surface brightness profiles for the system before (open circles) and after (solid circles) the relaxing run. The profile after the relaxing run is similar to the profile before. We also confirmed that all the properties presented in this paper are not changed after the relaxing run. Therefore, the properties at $z = 5.9$ are expected to be unchanged till $z = 0$. We present only the results from the data after the relaxing run in the next section.

The solid line in Figure 2 represents a King profile with the core radius, $r_{\rm c}$, and tidal radius, $r_{\rm t}$, same as the observed values in the Scl dSph, i.e. $r_{\rm c} = 0.12$ kpc and $r_{\rm t} = 1.6$ kpc. We assume the distance of the Scl dSph is 72 kpc (Kunkel & Demers, 1977, T04). The central surface brightness is normalized to roughly match with the simulated surface brightness profile. In the inner region, the simulated system has a similar profile to the observed profile of the Scl dSph, which means that the simulated galaxy has a similar core radius. In the outer region, the simulated galaxy has higher surface brightness compared to the King profile. Therefore, the tidal radius of the simulated galaxy is inconsistent with the observed one. However, our simulated galaxy is an isolated system, while the Scl dSph is a satellite galaxy of the Milky Way. We expect that if the simulated galaxy falls into a bigger host galaxy, the stars in the outer region are tidally stripped, and thus the tidal radius would depend on their environment, which could make the tidal radius of the simulated galaxy smaller and similar to the observed one. Here, we assume that such stripping does not change the properties of the inner region, and compare the properties of this isolated system with those of the Scl dSph.

The basic properties of the simulated galaxy are summarized in Table 1. In the next section, we compare our model results with the observational data of the Scl dSph in T04.

3. Results

Figure 3 shows the formation history of this galaxy. Although some minor mergers are involved, the system is forming through the smooth accretion. The lower panel of Figure 4 shows the virial mass evolution of the galaxy and building blocks which merge into the galaxies. The panel demonstrates that the main system experiences only two minor mergers (mass ratio

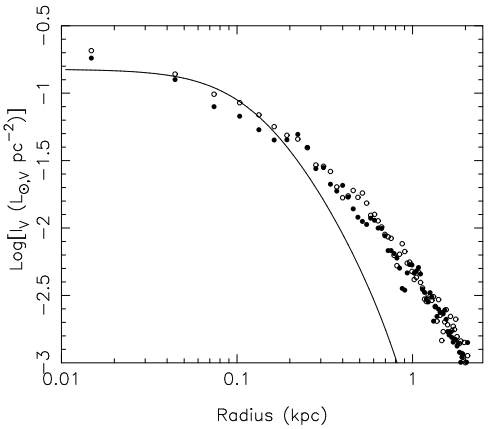

図 2: The V-band surface brightness profile from the simulation data before (open circles) and after (solid circles) the relaxing run (see text for details). The solid line presents a King profile with the core radius, $r_c = 0.12$ kpc, and tidal radius, $r_t = 1.6$ kpc.

表 1: Basic Model Results

M_{vir} ($M_\odot$)	r_{vir} (kpc)	$M_{gas}(< r_{vir})$ ($M_\odot$)	$M_{DM}(< r_{vir})$ ($M_\odot$)	$M_{star}(< r_{vir})$ ($M_\odot$)	M_V (mag)	T^a_{vir} (K)
5.1×10^7	1.9	3.5×10^5	5.0×10^7	1.9×10^5	−7.23	2.8×10^3

a Virial temperature calculated by $GM_{vir}\mu m_p/3k_B r_{vir}$ (Kitayama & Suto, 1996).

smaller than 0.4). The upper panel of Figure 4 shows the history of the star formation rate (SFR). In this galaxy, star formation starts at $z = 25.5$, and the SFR has a peak around $z = 15$. The $z = 17.8$ panel in Figure 3 shows that the gas is blown out and the heavy elements are distributed to the IGM. Our assumed SNe feedback (7.5×10^{50} erg per supernova which is chosen to reproduce the low metallicity of the Scl dSph) has a strong effect on the gas dynamics, and continuously blows out the gas from the system. However, the continuous gas accretion leads to further star formation, albeit at a somewhat lower rate. Figure 4 displays that star formation continuously occurs even around this blow-out phase. Nevertheless, star formation of this small system is strongly suppressed by SNe feedback, which helps to keep the stellar metallicity low, as seen in the age-metallicity relation shown in the right panel of Figure 5.

As described in Section 1, T04 found that the stars in the inner region have higher metallicity than those in the outer region. They split the two regions at the radius of about 0.25 kpc, and demonstrated that the metallicity distribution function (MDF) of stars in the inner (outer) region has a peak around [Fe/H]= −1.4 (−2.0). To compare with their result, Figure 6 shows the MDF for stars in the inner (R <0.25 kpc[1]) and outer (R>0.25 kpc) regions for our simulated galaxy. The MDF for the inner (outer) region of the simulated galaxy has a peak at [Fe/H]∼ −1.4 ([Fe/H]∼ −1.9), which is in good agreement with the observed MDFs in T04. Therefore, the simulated galaxy also show two distinct stellar populations.

We found that this is just due to the metallicity gradient in the system. Figure 5 shows the peak of the metallicity distribution at different radii gradually decreases, as the radius increases, i.e. there is a metallicity gradient in the simulated system. Since the metallicity gradient is steep

[1] Throughout this paper, R represents radius at an arbitrary projection, and we ignore the stars $R > 2.5$ kpc.

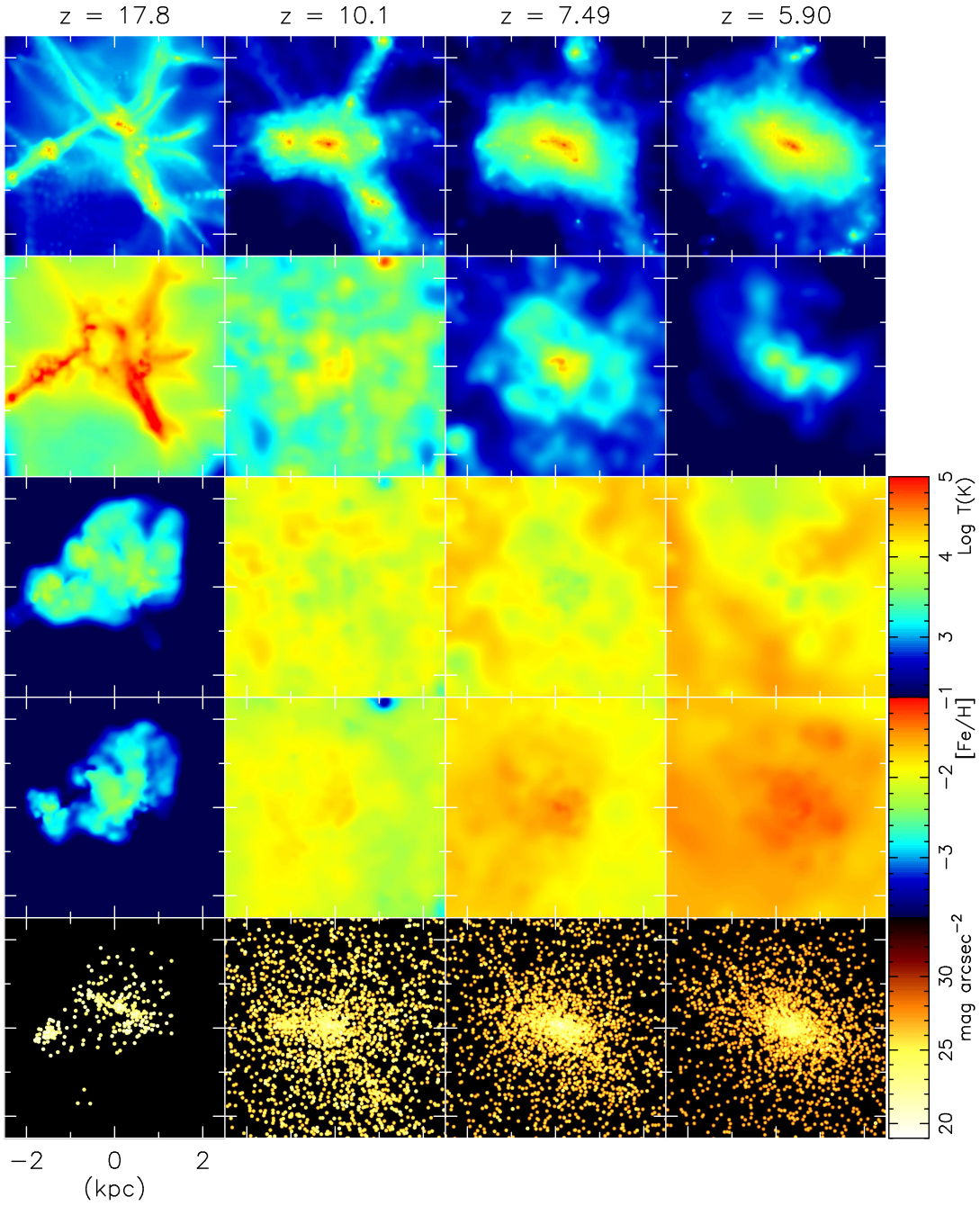

図 3: Evolution of the distributions of dark matter density (top), the gas density (2nd), the gas temperature (3rd), the iron abundance of gas (4th), and K-band (observed-frame) luminosity (bottom).

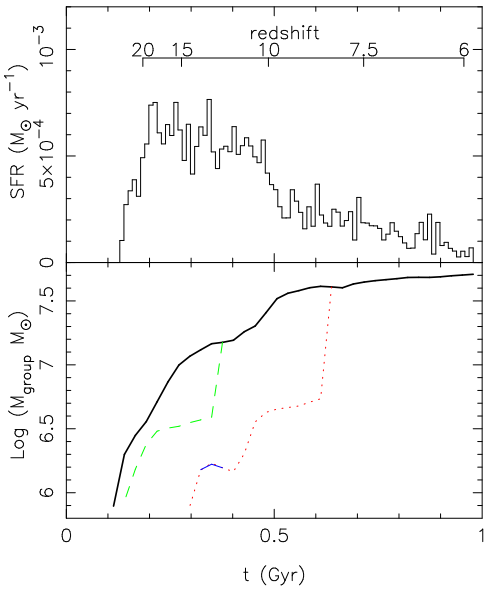

図 4: Time variation of the star-formation rate and the evolution of the virial mass of the progenitor halos. In the bottom panel, different styles of the lines (black thick-solid, red dotted, green dashed and blue thin-solid) indicate different halos. The connection between lines displays that two halos merge together. For example, the halo shown by red dotted line merges into the large halo described by black thick-solid line at $t \sim 0.64$ Gyr.

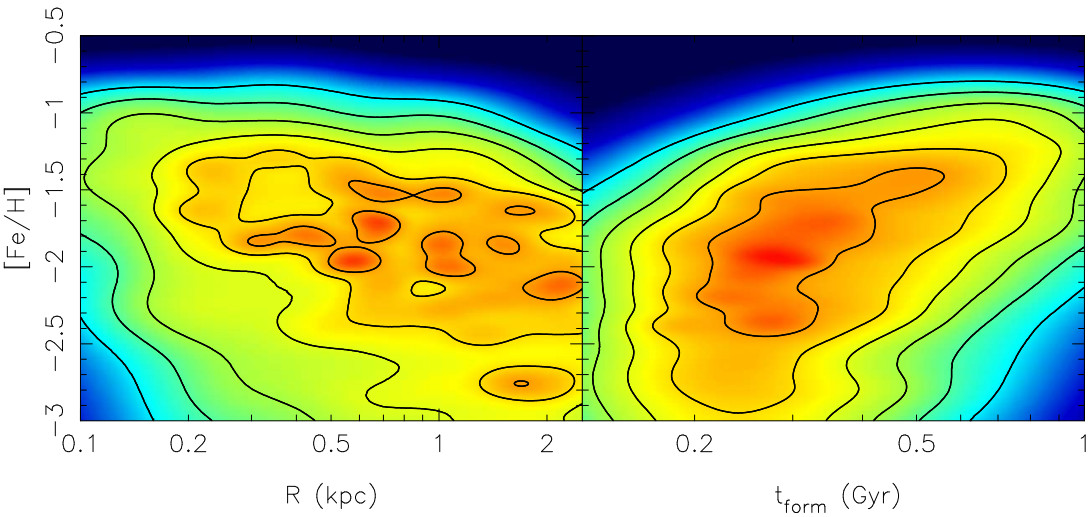

図 5: Smoothed stellar mass distribution in the [Fe/H] vs. radius plane (left) and in the [Fe/H] vs. formation time, t_{form}, plane, i.e. the age-metallicity relation (right).

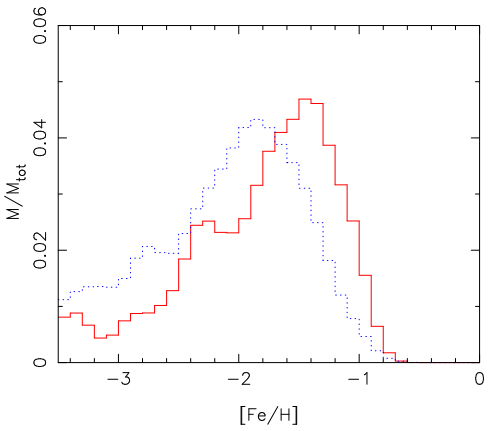

図 6: Metallicity distribution function of stars in the inner ($R < 0.25$ kpc: red solid histogram) and outer ($R > 0.25$ kpc: blue dotted histogram) region.

enough in the system, the MDF for the inner region moves toward higher [Fe/H], compared to the MDF for the outer region. This demonstrates that the steep metallicity gradient can make the two different chemical properties in the inner and outer regions.

Next, we analyze the kinematic properties. Figure 7 presents the velocity dispersion at different radii for the low ([Fe/H]< -1.7) and high ([Fe/H]> -1.7) metallicity stars. This velocity dispersion is obtained by taking the line-of-sight velocity dispersion of stars within annuli at different radii. To improve the statistics, we analyzed the line of sight profiles at 36 different projections, and obtained the mean values and dispersions, the latter for which are represented as error-bars in the figure. Figure 7 also shows the observed velocity dispersion of the low ([Fe/H]< -1.7) and high ([Fe/H]> -1.7) metallicity stars in T04. Within the radius of about 0.6 kpc, the observational data show that the velocity dispersion of the high metallicity stars is lower than that of the low metallicity stars[2] . In other words, the two different metallicity components also have distinctive dynamical properties. Our simulation results also show the same trend. Although the difference is small, the difference is significant and more than twice that of the dispersions shown as the error-bars in the inner region.

Our simulation demonstrates that a system formed at a high redshift can reproduce the two stellar populations whose chemical and dynamical properties are distinctive. However, the simulated galaxy shows some inconsistent results with the observed properties of the Scl dSph. First, compared with Figure 3 of T04, the MDFs for both inner and outer regions of the simulated galaxy have a too long tail at lower [Fe/H]. In the observational data, there are no stars at [Fe/H]< -2.8, although T04 selected their samples from the limited region of the color-magnitude diagram, which might tend to exclude too low and too high metallicity stars. On the other hand, the simulated galaxy has a significant fraction of stars with such low metallicity. Next, Figure 7 also shows that the velocity dispersion of our simulated galaxy is too small compared with the observed values. In addition, Table 1 presents that the V-band magnitude of the simulated galaxy ($M_V = -7.23$), which is also small, compared with the luminosity of the Scl dSph ($M_V = -10.7$). These are problems of our current model, which are required to

[2] Note that T04 mentioned that in the region outside of the radius of 0.6 kpc, the number of the high metallicity stars are too small.

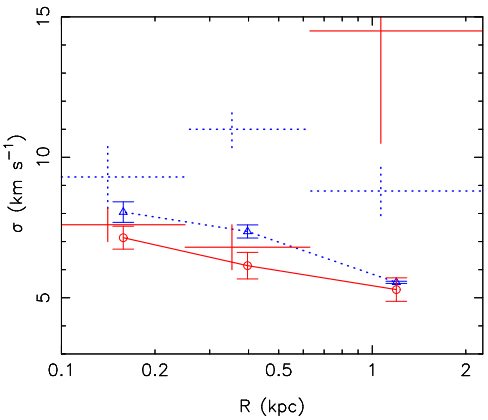

図 7: Velocity dispersion profile of high ([Fe/H]> -1.7: red circles connected with solid line) and low ([Fe/H]< -1.7: blue triangles connected with dotted line) metallicity stars. The error-bars represent the dispersions from the measurements at the different projections. The observational data in T04 are also shown as the red solid (for [Fe/H]> -1.7) and blue dotted (for [Fe/H]< -1.7) crosses, where the horizontal-bar corresponds to the radial range, and the vertical-bar corresponds to their dispersion. The vertical-bars are plotted with an offset, for clarity.

be solved in a future study, and we will discuss possible solutions in the next section.

We also analyzed the abundance ratio of [N/O] against [O/H], and found an interesting feature. Figure 8 demonstrates that there is a visible trend that [N/O] decrease from [N/O]$= 2$ to ~ 0 as [O/H] increase from [O/H]$= -4$ to -1.5. The middle panel of the figure also shows that high [N/O] are seen in the stars formed around $t = 0.3$ Gyr, and the stars born at later epochs have lower [N/O]. This high [N/O] comes from the stars with the mass between 4 and 8 $M_\odot$ whose lifetime is around 0.1 Gyr (right panel of Figure 8). To make the contribution from such intermediate mass stars important, it is required to suppress the contribution from the higher mass stars whose [N/O] are lower and whose lifetime is shorter. As seen in Figure 3, the enriched gas is blown out at a high redshift around $z = 17$, due to the strong feedback by SNe II and relatively shallow potential of the system at such a high redshift. As a result, the chemical enrichment by the massive stars, i.e. SNe II, becomes less important, and enrichment from the intermediate mass stars becomes relatively more important. As the system gets bigger and their gravitational potential can bound the gas enriched by SNe II, [N/O] starts decreasing. Testing this trend of [N/O] in dSphs would be interesting. To our knowledge, the nitrogen abundance has not been observed in the dSphs. On the other hand, the intermediate mass stars are also expected to be progenitors of s-process elements. Recent observational studies (e.g., Sadakane et al., 2004; McWilliam & Smecker-Hane, 2005) suggest that the s-process elements are enhanced in the dSphs. This might be explained by the process that the SNe II enriched gas is preferentially blown out from the system, and the enrichment by the intermediate mass stars is more important in the dSph. Interestingly, Smecker-Hane & McWilliam (2002); McWilliam & Smecker-Hane (2005) show that the s-process elements are more enhanced in higher metallicity stars in the Sagittarius dSph. In addition, Sadakane et al. (2004) found a very metal poor star ([Fe/H]$= -2.7$) which has anomalously low abundance of the s-process elements in the

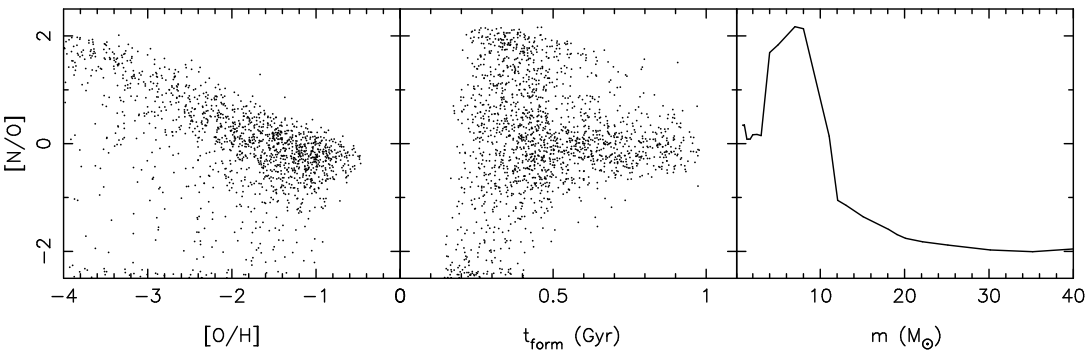

図 8: *Left*: [N/O] as a function of [O/H] for star particles within $R = 2.5$ kpc. *Middle*: [N/O] as a function of their formation epoch. *Right*: [N/O] yields as a function of the mass of the progenitor stars with metallicity of $Z/Z_\odot = 0.01$ (Woosley & Weaver, 1995; van den Hoek & Groenewegen, 1997).

Ursa Minor dSph. This may indicate a delay of s-process elements enrichment, because s-process elements come from relatively low mass ($1.5 \sim 3$ $M_\odot$), i.e. long lifetime, stars (see also Lanfranchi et al., 2005).

4. Discussion and Conclusions

We have analyzed chemical and kinematic properties of a small systema which formed at a high redshift in the ΛCDM cosmological simulation. Our simulated galaxy shows that the higher metallicity ([Fe/H]> -1.7) stars have more centrally concentrated distribution and lower velocity dispersion, compared with the lower metallicity stars ([Fe/H]< -1.7). This trend is consistent with the observed trend in the Scl dSph reported in T04. Thus, we conclude that a survivor of a small system which formed at a high redshift can explain the observed stellar chemical and kinematic properties.

T04 claimed that this observed trend indicates that there are two distinct populations in the Scl dSph. They argue three possible mechanisms to explain the two populations. 1) Two episodes of star formation: The subsequent SNe feedback from the initial star formation blows out the gas and stops star formation temporally. After SNe feedback gets weaker, more metal-rich gas comes back and forms new generation of stars (Carraro et al., 2001). 2) External influences, such as minor mergers or accretion of additional gas at later epoch. 3) Selected heating by the UV background radiation: The radiation evaporates the outer layers of the gas preferentially, and star formation lasts longer in the inner region (Susa & Umemura, 2004). Figure 4 shows that our simulated galaxy does not have two episodes of star formation. In this study, we assume that there is no later minor merger or gas accretion after star formation is stopped at the high redshift, and star formation is abruptly terminated without any time delay depending on the radius. Thus, the formation history of our simulated galaxy does not correspond to any above scenario.

Figures 3 and 4 show that the simulated galaxy forms through the smooth accretion rather than major mergers. It is known that such smooth accretion of the dissipative gas component leads to the higher metallicity for the gas in the inner region, because the gas which dissipatively

accrets into the inner region are enriched by the stars in the outer region as well as the stars in the inner region where the stellar density is higher. This is the same mechanism as what is suggested to explain the metallicity gradient for larger spheroidals, i.e. normal elliptical galaxies (Larson, 1974). In fact, Figure 5 shows a metallicity gradient in the simulated system. Hence, our simulation demonstrates that for a small system, which stopped star formation at a high redshift, it is possible to have a metallicity gradient, which can explain the *apparent* two distinct populations observed in the dSph Scl stars. Note that the metallicity gradient has to be steep, to make such difference in the inner and outer region. However, here we also note that our simulation result does not rule out alternative scenairos to explain the observed two populations, such as those discussed in T04.

Unfortunately, some properties of our simulated galaxy are inconsistent with those observed in the Scl dSph. Figure 6 shows that in both inner and outer region there are significant amount of stars which have extremely low metallicity. Another problem in our simulated galaxy is too less luminous and too small velocity dispersion. We have tried the different parameter sets of models for star formation and SNe feedback. However, we found that to keep metallicity as low as what is observed, the strong SNe feedback that leads to the low efficiency of star formation is required, which makes it difficult to produce enough stars at a high redshift. A solution would be that they were more massive. The virial mass of our galaxy is 5×10^7 $M_\odot$ at $z \sim 6$. The dynamical analysis of the dSphs suggests that their mass to light ratio is more than hundred (e.g., Kleyna et al., 2001), which suggests that the total mass of the Scl dSph is more than 10^8 $M_\odot$. If the system is big enough, they might be able to continue a low level of star formation even after the re-ionization in the inner region along the scenario 3) described above.

Our simulation demonstrates that the recently available detailed properties of the observed dSph provide invaluable information about their formation history. Our current cosmological simulations obviously miss, or oversimplify, some important physics. For example, our SNe feedback model is too simple, and/or the resolution of our simulation is not good enough to describe SNe feedback, although the present study shows that the effect of SNe would be crucial to explain the observed properties of the dSph. Also, the IMF might depend on the physical condition of the progenitor gas, such as metallicity. In addition, our simulation ignores the radiative transfer effects, such as radiative heating and pressure. The strong light from new born stars would suppress cooling of the surrounding gas, which would be important in the small system. Nevertheless, the dSph is a good laboratory for studying the physical process of the galaxy formation. We hope that our present study would be a good starting point to test the formation scenario of the dSph, comparing the detailed observation with chemo-dynamical galaxy formation models.

参考文献

Arimoto, N., & Yoshii, Y. 1987, A&A, 173, 23

Baade, W. 1944, ApJ, 100, 137

Bertschinger, E. 2001, ApJS, 137, 1

Carraro, G., Chiosi, C., Girardi, L., & Lia, C. 2001, MNRAS, 327, 69

Dekel, A., & Silk, J. 1986, ApJ, 303, 39

Efstathiou, G. 1992, MNRAS, 256, 43P

Gallagher, J. S., & Wyse, R. F. G. 1994, PASP, 106, 1225

Kawata, D., & Gibson, B. K. 2003a, MNRAS, 340, 908

—. 2003b, MNRAS, 346, 135

Kitayama, T., & Suto, Y. 1996, ApJ, 469, 480

Kleyna, J. T., Wilkinson, M. I., Evans, N. W., & Gilmore, G. 2001, ApJ, 563, L115

Kodama, T., & Arimoto, N. 1997, A&A, 320, 41

Kunkel, W. E., & Demers, S. 1977, ApJ, 214, 21

Lanfranchi, G. A., Matteucci, F., & Cescutti, G. 2005, ArXiv Astrophysics e-prints

Larson, R. B. 1974, MNRAS, 166, 585

McWilliam, A., & Smecker-Hane, T. A. 2005, in ASP Conf. Ser. 336: Cosmic Abundances as Records of Stellar Evolution and Nucleosynthesis, 221–+

Mo, H. J., & White, S. D. M. 1996, MNRAS, 282, 347

Ricotti, M., & Gnedin, N. Y. 2005, ApJ, 629, 259

Sadakane, K., Arimoto, N., Ikuta, C., Aoki, W., Jablonka, P., & Tajitsu, A. 2004, PASJ, 56, 1041

Smecker-Hane, T. A., & McWilliam, A. 2002, astro-ph, 0205411

Spergel, D. N., Verde, L., Peiris, H. V., Komatsu, E., Nolta, M. R., Bennett, C. L., Halpern, M., Hinshaw, G., Jarosik, N., Kogut, A., Limon, M., Meyer, S. S., Page, L., Tucker, G. S., Weiland, J. L., Wollack, E., & Wright, E. L. 2003, ApJS, 148, 175

Susa, H., & Umemura, M. 2004, ApJ, 600, 1

Tolstoy, E., Irwin, M. J., Helmi, A., Battaglia, G., Jablonka, P., Hill, V., Venn, K. A., Shetrone, M. D., Letarte, B., Cole, A. A., Primas, F., Francois, P., Arimoto, N., Sadakane, K., Kaufer, A., Szeifert, T., & Abel, T. 2004, ApJ, 617, L119

van den Hoek, L. B., & Groenewegen, M. A. T. 1997, A&AS, 123, 305

White, S. D. M., & Rees, M. J. 1978, MNRAS, 183, 341

Woosley, S. E., & Weaver, T. A. 1995, ApJS, 101, 181